Extension of the cone-beam CT field-of-view using two short scans with displaced centers of rotation

Gabriele Belotti, Simon Rit, Guido Baroni

Gabriele Belotti, Simon Rit, Guido Baroni, "Extension of the cone-beam CT field-of-view using two short scans with displaced centers of rotation," Proc. SPIE 12304, 7th International Conference on Image Formation in X-Ray Computed Tomography, 123040E (17 October 2022); doi: 10.1117/12.2646384

SPIE.

Event: Seventh International Conference on Image Formation in X-Ray Computed Tomography (ICIFXCT 2022), 2022, Baltimore, United States

Extension of the cone-beam CT field-of-view using two short scans with displaced centers of rotation

Gabriele Belotti[a*], Simon Rit[b], and Guido Baroni[a,c]

[a]Politecnico di Milano, CartCasLab; DEIB, Milan, Italy
[b]Université de Lyon, CREATIS; CNRS UMR5220; Inserm U1294; INSA-Lyon; Université Lyon 1; Centre Léon Bérard, Lyon, France
[c]Bioengineering Unit, CNAO Foundation, Pavia, Italy

ABSTRACT

A robotic cone-beam computed tomography (CT) scanner has inherent advantages. In particular, it enables source and detector trajectories capable of extending the field-of-view (FOV) of the reconstructed CT images, where the FOV is defined as the region in the source trajectory plane for which all ray lines are acquired (at any position and direction in this plane). Previous extensions of the FOV used an offset detector or a displaced center of rotation and a single full 360° scan. However, due to limitations in the conventional range of motion inside the treatment room to avoid collisions, some systems can only perform short scans. This paper investigates a new approach to FOV extension for an existing system by adapting the FOV extension to two complementary short scans with displaced centers of rotation. We validate this approach on numerical simulations of the Forbild thorax phantom.

1. INTRODUCTION

Cone-beam computed tomography (CBCT) is a common solution to provide in-room imaging in various forms of radiotherapy. Several commercial solutions are available, often as an imager mounted on the gantry of a linear accelerator. At the same time, custom solutions exist as well, in particular for hadrontherapy.[1] The National Center for Oncological Hadrontherapy (CNAO, Pavia, Italy) employs such a scanner: a custom CBCT scanner mounted on a Kawasaki robotic manipulator.[2] It provides high geometric reproducibility and is employed for both individual X-ray radiographs and CBCT acquisitions inside the treatment room before the delivery of the treatment fraction. The device was primarily intended for correcting the patient setup based on registration of the bony anatomy and cannot produce a sufficiently wide field-of-view (FOV) to avoid data truncation when targeting wider locations, e.g. the abdomen or the thorax. In this work, the FOV is defined as the region in the source trajectory plane for which all ray lines are acquired (at any position and direction). Adaptive radiotherapy using the acquired CBCT images is being investigated, but it is of clinical interest to accurately reconstruct complete axial slices in wide locations for qualitative and dosimetric assessments of interfractional variations. Like most CBCT scanners with a fixed flat panel detector (FPD), the *conventional geometry* of the system is such that for all source positions, the midline, defined by the point source and the center of the detector, is orthogonal to the rotation axis and intersects it at the center of the source trajectory.[3] Axial FOV enlargement is typically achieved through a technique called half fan, suitable for filtered backprojection (FBP) reconstruction.[4] Mechanically, half fan requires a detector capable of transverse displacements and an adjustable X-ray source collimation. Both features are not available in the aforementioned CNAO CBCT scanner. A feasible alternative is to perform a complete displaced center of rotation (DCoR) scan with a fixed tilt of the detector. This consists of a 360° scan where the midline is offset w.r.t. the axis of rotation. This offset can be realized by the CNAO CBCT scanner while the relative positions of the source and detector are unchanged and the same collimation can be used. Previous works dealt with DCoR and aimed at correcting it as a misalignment.[5] Instead, we would like to use this geometry to enlarge the reconstructed FOV, as in Ref. 3. Such a trajectory is compatible with robotic manipulators as the one of the CNAO CBCT scanner and is easily programmable in the robot controller. However, bulky hardware in the treatment room limits the sampling arc of the C-arm to 220°. The objective of this work is to exploit a couple of short scans[6] with complementary offset centers of rotation to obtain the same FOV as a single full 360° DCoR scan would produce.

*Corresponding author email: gabriele.belotti@polimi.it

7th International Conference on Image Formation in X-Ray Computed Tomography, edited by Joseph Webster Stayman, Proc. of SPIE Vol. 12304, 123040E
 · 0277-786X · doi: 10.1117/12.2646384

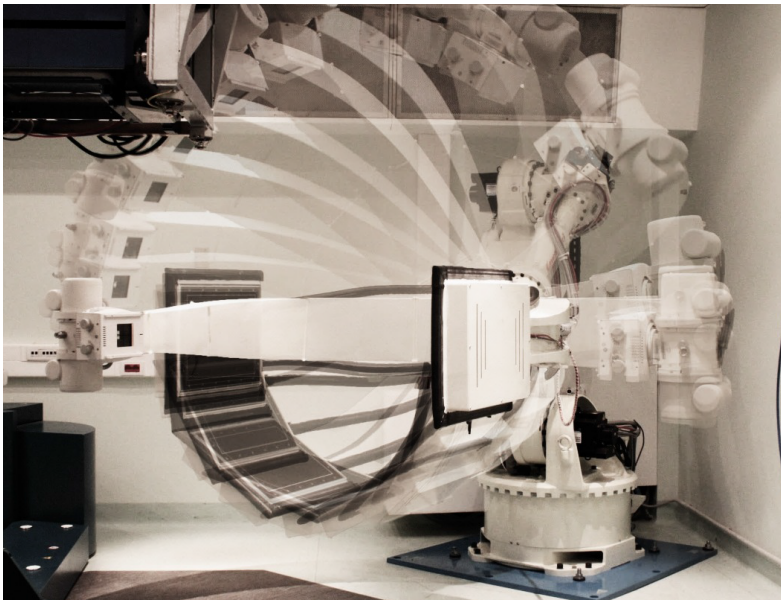

Figure 1. Short time-lapse depicting conventional motion of custom in-room CBCT imaging system at CNAO. On the bottom left, one can observe the base of the robotic couch, which prevents the full rotation of the C-arm.

2. MATERIALS AND METHODS

2.1 Circular geometry with displaced center of rotation

We examine the scanner geometry in the central plane $z = 0$ containing the trajectory of the source S. The source and detector are attached to a C-arm which rotates around the isocenter I. We note SID and SDD the source-to-isocenter and source-to-detector distances which are fixed by construction. In the conventional operation, the source and detector rotate on a circle centered on I which is static. We note β the gantry angle between the y-axis and the midline (defined by the source S and the isocenter I).

The DCoR geometry makes use of the possibility given by the robotic manipulator to modify the position of I during the system rotation. With respect to the conventional operation, both the source and the FPD are offset from the center O in a direction orthogonal to the midline (and therefore parallel to the detector) as shown in Figure 2. We note τ the angle between the source-center line and the midline which is also the tilt angle between a conventional detector (orthogonal to the source-center line) and the DCoR detector. Like in Ref. 5 and unlike Ref. 3, τ is constant w.r.t. the gantry angle β. The angle τ is positive when I is on the positive side of the x-axis at gantry angle $\beta = 0$ as in Figure 2. The offset of the isocenter w.r.t. to the conventional geometry, i.e. the isocenter-to-center distance, is $R_I = \text{SID}|\tan\tau|$.

The source trajectory is still a circle, centered on O and defined by $S(\tau, \beta) = R_S(-\sin(\beta - \tau), \cos(\beta - \tau), 0)$, where $R_S = \sqrt{\text{SID}^2 + R_I^2}$ is the radius of the circle. The isocenter trajectory is also a circle of center O such that $I(\beta) = R_I(\cos\beta, \sin\beta, 0)$. The conventional geometry is when $\tau = 0$, i.e. when $R_I = 0$ and $R_S = \text{SID}$. We note $\alpha_\tau = \alpha + |\tau|$ the large fan angle captured by the detector in the central plane with $\alpha = \arctan(N_u\Delta_u/2\ \text{SDD})$ the fan angle captured by the detector w.r.t. the midline (Figure 2), N_u the number of pixels of the detector in the transaxial direction and Δ_u their spacing. If $|\tau| < \alpha$, the source-to-center line hits the detector and the DCoR strategy could achieve exact reconstruction in the central slice of the FOV with radius $R_{\text{FOV}} = R_S \sin\alpha_\tau$. This is normally done with a full 360° scan but we propose to combine it with short scans.

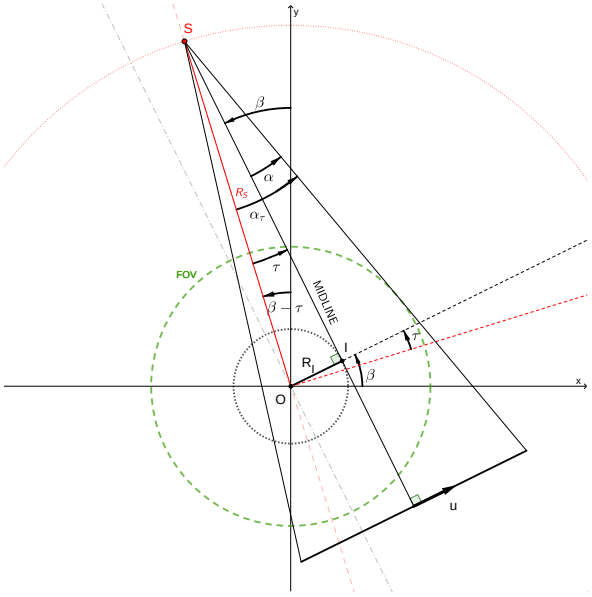

Figure 2. Circular geometry defined as *displaced center-of-rotation* (DCoR) in the central plane. The FPD and source S are bound together while S travels the circle with radius R_S. The midline is offset from the center O of the source trajectory.

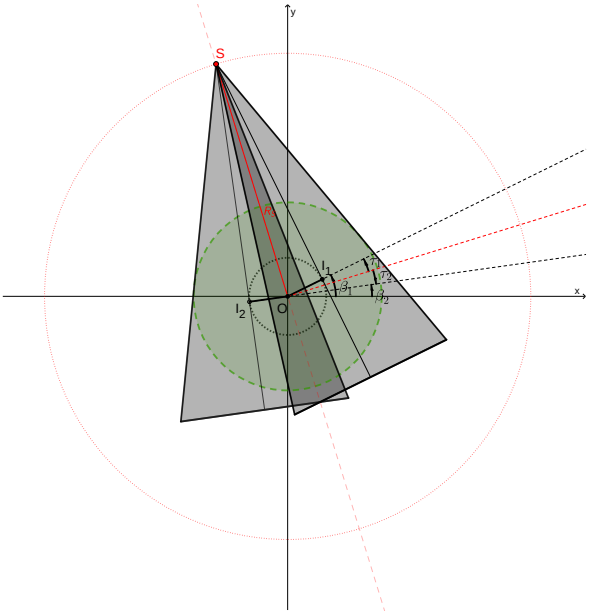

Figure 3. Illustration of two projections of two complementary scans with τ_1 and $\tau_2 = -\tau_1$, with gantry angle $\beta_2 = \beta_1 - 2\tau_1$ such that the source is at the same position $S(\tau_1, \beta_1, 0) = S(\tau_2, \beta_2, 0)$ in the two arcs.

2.2 Short scan

Let g_τ be the set of cone-beam projections acquired for a given DCoR geometry with an angle τ defined by the line integral

$$g_\tau(\beta, u, v) = \int_{\mathcal{L}(\tau,\beta,u,v)} f(x)\mathrm{d}x \tag{1}$$

where $\mathcal{L}(\tau, \beta, u, v)$ is the line defined at gantry angle β and tilt angle τ by the source position $S(\tau, \beta)$ and the position of the detector pixel with coordinates (u, v).

If the projections were untruncated with a full fan $\alpha_u \in [-\alpha_\tau, \alpha_\tau]$ with $\alpha_u = \tau + \arctan(u/\mathrm{SDD})$, a short scan of $\pi + 2\alpha_\tau$ would be sufficient to reconstruct from divergent rays in the central plane using Parker pre-reconstruction weights[6]

$$w_P(\beta, u, v) = \begin{cases} \sin^2\left(\frac{\pi}{4}\frac{\beta}{\alpha_\tau - \alpha_u}\right) & \text{if } 0 \le \beta \le 2\alpha_\tau - 2\alpha_u, \\ \sin^2\left(\frac{\pi}{4}\frac{\pi + 2\alpha_\tau - \beta}{\alpha_\tau + \alpha_u}\right) & \text{if } \pi - 2\alpha_u \le \beta \le \pi + 2\alpha_\tau, \\ 1 & \text{otherwise.} \end{cases} \tag{2}$$

In Ref. 3, the authors provide an adaptation of the FDK algorithm[7] to a full scan DCoR geometry and we note $\mathcal{R}_\tau$ its application to a short scan:

$$f \simeq \mathcal{R}_\tau \left\{ w_P g_\tau \right\}. \tag{3}$$

This short scan DCoR reconstruction is only exact in the central slice and approximate elsewhere due to the cone-beam artifact stemming from incomplete data with a circular source trajectory.

2.3 Complementary short scans

We note that for two scans with opposite offsets τ_1 and $\tau_2 = -\tau_1$, the source rotates on the same circle since $S(\tau_1, \beta) = S(\tau_2, \beta - 2\tau_1)$. We therefore acquire the corresponding cone-beam projections g_1 and g_2 for the same

arc of source trajectory using the two sets of gantry angle $B_1 = [\tau_1, \pi + 2\alpha_{\tau_1} + \tau_1]$ and $B_2 = [\tau_2, \pi + 2\alpha_{\tau_2} + \tau_2]$ which measure the same line integrals in the central plane

$$g_1(\beta, u, 0) = g_2(\beta - 2\tau_1, \mathrm{SDD}\tan(\alpha_u - \tau_2), 0). \tag{4}$$

We refer to this composition of trajectories as *complementary displaced centers-of-rotation* (C-DCoR). The detectors are however in different positions with a small overlap (Figure 3). We follow the approach of Refs. 4 and 6 to manage redundancies with the weights

$$w_i(\beta, u, v) = \begin{cases} \frac{1}{2}\left(\mathrm{sign}\,\tau_i \sin\left(\frac{\pi\alpha_u}{2(\alpha - |\tau_i|)}\right) + 1\right) & \text{if } |\alpha_u| < \alpha - |\tau_i|, \\ 1 & \text{otherwise,} \end{cases} \tag{5}$$

which are derived from the displaced detector weights of Ref. 8. We obtain the reconstruction formula

$$f \simeq \mathcal{R}_{\tau_1}\left\{w_P w_1 g_1\right\} + \mathcal{R}_{\tau_2}\left\{w_P w_2 g_2\right\}. \tag{6}$$

It can be shown that the reconstruction is exact in the central plane, as in (3). The result of (3) is however different in other planes but previous investigations have shown that the effect of the tilt is limited compared to the cone-beam artifacts in these planes.[3]

3. EXPERIMENTS

The proposed C-DCoR trajectories have been tested on simulated projections of a Forbild thorax phantom using RTK.[9] Geometrical parameters of the simulations mimick the CNAO scanner with SID = 1100 mm and SDD

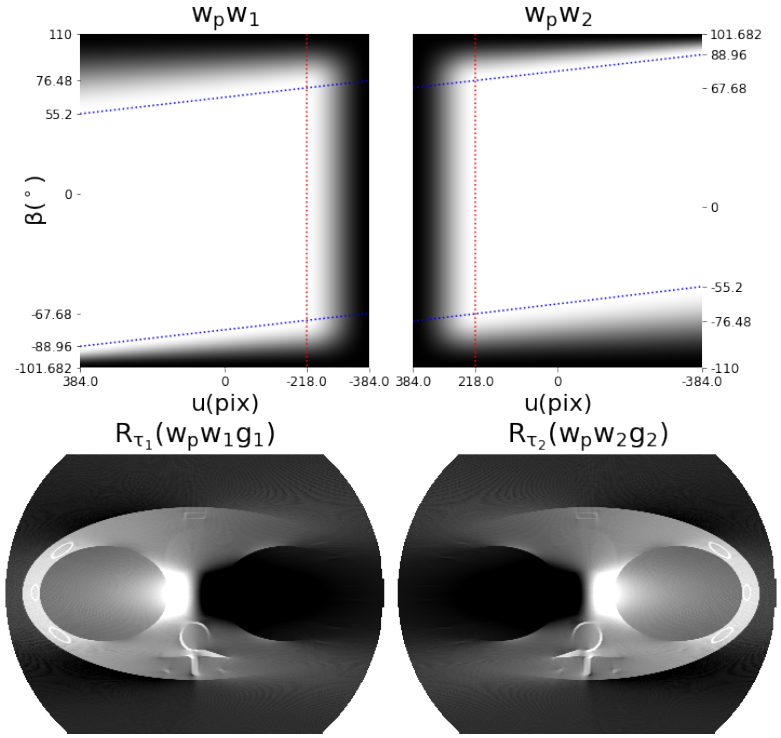

Figure 4. Top row shows the weight maps $w_p w_1$ and $w_p w_2$ (grayscale range $[0, 1]$) for the two fan-beam sinograms of the central slice. Vertical dotted red lines indicate the limit for the offset detector weights w_1 and w_2 (Equation 5). Slanted blue dotted lines indicate the limits for Parker short scan weights (Equation 2). Bottom row shows partial reconstructions $\mathcal{R}_{\tau_1}(w_p w_1 g_1)$ and $\mathcal{R}_{\tau_2}(w_p w_2 g_2)$, the sum of which gives the axial slice shown at the left of the second row in Figure 5. The grayscale range is $[-740, 920]$ HU.

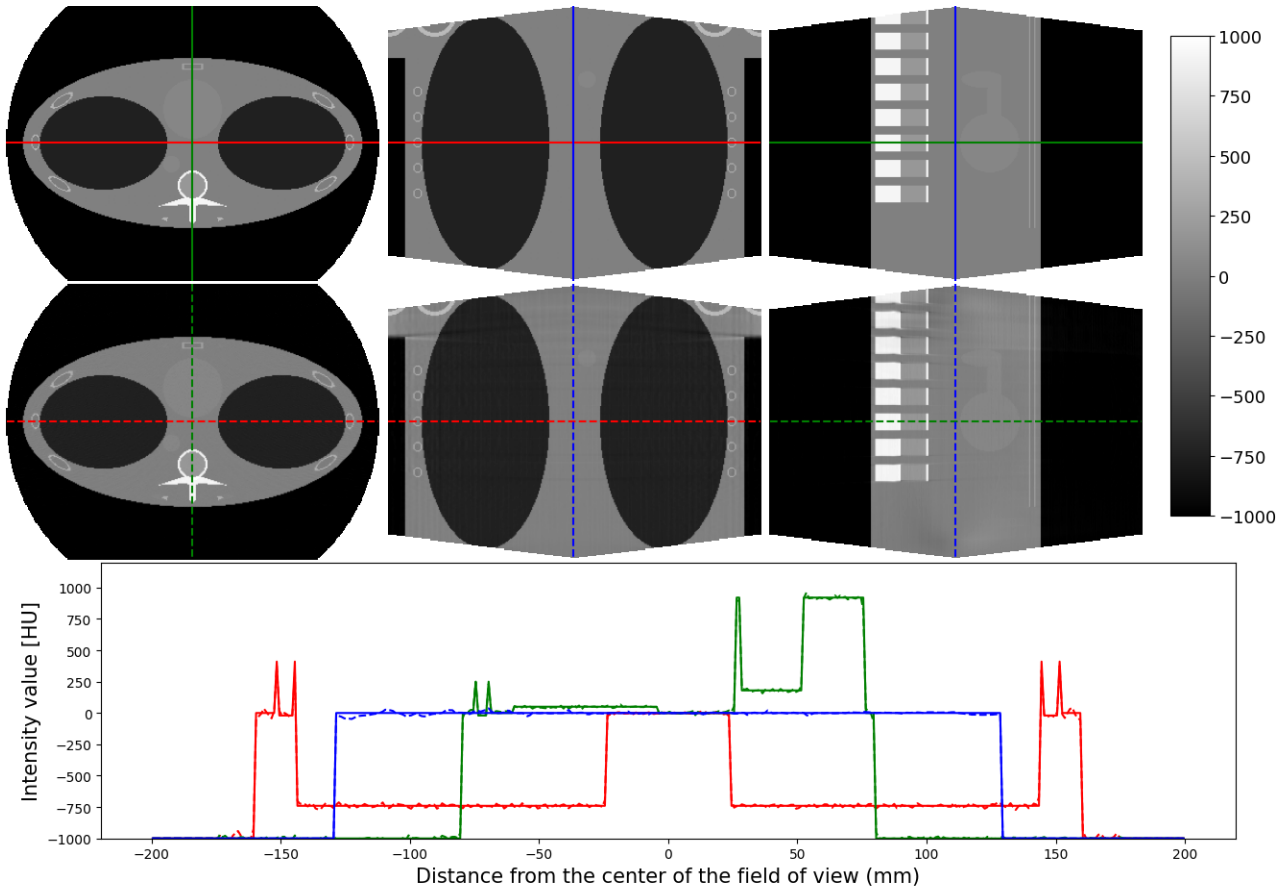

Figure 5. Top row shows central slices (axial, coronal, sagittal) extracted from the Forbild reference volume, with grayscale in Hounsfield Units. Central row shows the same slices from a C-DCoR image with an offset $R_I = 80$ mm. Grayscale level and window are set to 0 and 2000 HU, where -740 HU is the value in the lung and 920 HU is the vertebrae density. Note that axial slices are cropped in the antero-posterior direction for optimal display. Colored lines indicate where the intensity profiles (bottom row) have been evaluated.

$= 1600$ mm. The detector has isometric spacing $\Delta_u = \Delta_v = 0.388$ mm and size $N_u \times N_v = 768 \times 1024$ pixels; we therefore have $\alpha = 5.32°$. We set $\tau_1 = -\tau_2 = 4.159°$ which results in $R_I = 80$ mm and $R_S = 1102.91$ mm. The same arc of the circle trajectory is covered with $B_1 \simeq [-102°, 110°]$ and $B_2 \simeq [-110°, 102°]$, which is larger than $180° + 2\alpha_\tau \simeq 199°$ and accounted for in the redundancy weights w_s (by replacing α_τ by half the scan range minus π in Ref. 2).

The reconstructed DCoR scans have a FOV diameter of 363 mm instead of 204 mm for the conventional geometry. The Forbild phantom is isometrically rescaled 0.8 times such that the thorax ellipse semi-minor and semi-major axes are 80 mm and 160 mm and fit in the DCoR FOV. The phantom is centered on O and 400 projections are generated along each complementary scan. The reconstructed scans have size $400 \times 400 \times 400$ pixels with a resolution of $1 \times 1 \times 1$ mm.

4. RESULTS

The weight maps $w_P w_1$ and $w_P w_2$ and the partial reconstructions $\mathcal{R}_{\tau_1}\{w_P w_1 g_1\}$ and $\mathcal{R}_{\tau_2}\{w_P w_2 g_2\}$ are displayed in the central slice along with the corresponding weight maps in Figure 4. The resulting phantom reconstruction is qualitatively compared to the reference phantom in Figure 5. The images are masked to the FOV of the C-DCoR scan. In the latter, artifacts caused by strong attenuation in high density vertebrae along the z axis are visible in the sagittal plane. Intensity profiles are extracted from the middle of each slice along the colored lines

in Figure 5 in the same figure. The difference between the reference image and the reconstructed image resulted in a mean absolute error (MAE) of 20.5(±24.5) HU inside the FOV. Slightly worse results are obtained when simulating and reconstructing a complete 400 projections half fan acquisition with a 130 mm detector offset with a MAE of 27.6(±25.5) HU (image not shown). Finally, we find equivalent results when simulating and reconstructing a conventional geometry acquisition with a large panel (1536 × 1024 pixels) on the same source trajectory with a MAE of 20.6(±24.0) HU (image not shown).

5. DISCUSSION AND CONCLUSIONS

We successfully developed a reconstruction algorithm to extend the FOV of the CNAO scanner. The C-DCoR acquisition can nearly double the FOV diameter. The method requires two short scans with a short movement of the isocenter and detector between the scans to ensure that the same source trajectory arc is imaged twice with different detector positions. With these arcs, we are able to produce CBCT images of similar quality as conventional short scan or displaced detector CBCT images. Most discrepancies in the reconstructed C-DCoR are caused by the phantom vertebrae and seem to be linked to the cone angle of incident X-rays. Physical effects such as scatter or geometrical fluctuations remain to be assessed on real data.

REFERENCES

[1] Landry, G. and Hua, C. H., "Current state and future applications of radiological image guidance for particle therapy," *Medical Physics* **45**(11), e1086–e1095 (2018).

[2] Fattori, G., Riboldi, M., Pella, A., Peroni, M., Cerveri, P., Desplanques, M., Fontana, G., Tagaste, B., Valvo, F., Orecchia, R., et al., "Image guided particle therapy in CNAO room 2: implementation and clinical validation," *Physica Medica* **31**(1), 9–15 (2015).

[3] Rit, S., Clackdoyle, R., Keuschnigg, P., and Steininger, P., "Filtered-backprojection reconstruction for a cone-beam computed tomography scanner with independent source and detector rotations," *Medical Physics* **43**(5), 2344–2352 (2016).

[4] Cho, P. S., Rudd, A. D., and Johnson, R. H., "Cone-beam CT from width-truncated projections," *Computerized Medical Imaging and Graphics* **20**(1), 49–57 (1996).

[5] Gullberg, G. T., Crawford, C. R., and Tsui, B. M., "Reconstruction algorithm for fan beam with a displaced center-of-rotation," *IEEE Transactions on Medical Imaging* **5**(1), 23–29 (1986).

[6] Parker, D. L., "Optimal short scan convolution reconstruction for fan beam CT," *Medical Physics* **9**(2), 254–257 (1982).

[7] Feldkamp, L. A., Davis, L. C., and Kress, J. W., "Practical cone-beam algorithm," *Journal of the Optical Society of America A* **1**(6), 612–619 (1984).

[8] Wang, G., "X-ray micro-CT with a displaced detector array," *Medical Physics* **29**(7), 1634–1636 (2002).

[9] Rit, S., Oliva, M. V., Brousmiche, S., Labarbe, R., Sarrut, D., and Sharp, G. C., "The Reconstruction Toolkit (RTK), an open-source cone-beam CT reconstruction toolkit based on the Insight Toolkit (ITK)," in [*Journal of Physics: Conference Series*], **489**(1), 012079, IOP Publishing (2014).